

Anna Yesypenko and Per-Gunnar Martinsson
University of Texas at Austin

Abstract: The paper describes a sparse direct solver for the linear systems that arise from the discretization of an elliptic PDE on a rectangular domains. The scheme decomposes the domain into thin subdomains, or “slabs”. Within each slab, a local factorization is executed that exploits the geometry of the local domain. A global factorization is then obtained through the LU factorization of a block-tridiagonal reduced system. The general two-level framework is easier to implement and optimize for modern latency-bound architectures than traditional multi-frontal schemes based on hierarchical nested dissection orderings. The solver has complexity $O(N^{5/3})$ for the factorization step, and $O(N^{7/6})$ for each solve once the factorization is completed.

The solver described is compatible with a range of different local discretizations, and numerical experiments demonstrate its high performance for standard finite difference discretizations on a regular grid. The technique becomes particularly efficient when combined with very high-order convergent multi-domain spectral collocation schemes. With this discretization, a Helmholtz problem on a domain of size $1000\lambda \times 1000\lambda$ (for which $N=100M$) is solved in 15 minutes to 6 correct digits on a high-powered desktop.

1. INTRODUCTION

1.1. **Problem setup.** We present a direct solver for boundary value problem of the form

$$(1) \quad \begin{cases} \mathcal{A}u(x) = f(x), & x \in \Omega, \\ u(x) = g(x), & x \in \Gamma, \end{cases}$$

where \mathcal{A} is a second order elliptic differential operator, and Ω is a rectangular domain in two dimensions with boundary Γ . The method works for a broad range of constant and variable coefficient differential operators, but is particularly competitive for problems with highly oscillatory solutions that are difficult to pre-condition. For the sake of concreteness, we will focus on the case where \mathcal{A} is a variable coefficient Helmholtz operator

$$(2) \quad \mathcal{A}u(x) = -\Delta u(x) - \kappa^2 b(x)u(x),$$

where κ is a reference (“typical”) wavenumber, and where $b(x)$ is a smooth non-negative function. Upon discretizing (1), one obtains a linear system

$$(3) \quad \mathbf{A}u = \mathbf{f},$$

involving a sparse coefficient matrix. Our focus is on efficient algorithms for directly building an invertible factorization of the matrix \mathbf{A} . We specifically consider two different discretization schemes, first a basic finite difference scheme with second order convergence, and then a high (say $p = 20$) order multidomain spectral collocation scheme [26, Ch. 25]. However, the techniques presented can easily be used with other (local) discretization schemes such as finite element methods.

1.2. **Overview of proposed solver.** The solver presented is based on a decomposition of the computational domain into thin “slabs”, as illustrated in Figure 1a. Unlike previously proposed sweeping preconditioner schemes [13, 15, 32], our objective is to directly factorize the coefficient matrix, or at least compute a factorization that is sufficiently accurate that it can handle problems involving strong backscattering.

To describe how the solver works, let us consider a simple model problem where the PDE is discretized using a standard five-point finite difference stencil on a uniform grid such as the one shown in Figure 1a. The nodes in the grid are arranged into slabs of width b , and are ordered as shown in Figure 1a, resulting in a coefficient matrix \mathbf{A} with the block diagonal sparsity pattern shown in Figure 1c. The factorization of \mathbf{A} then proceeds through two stages.

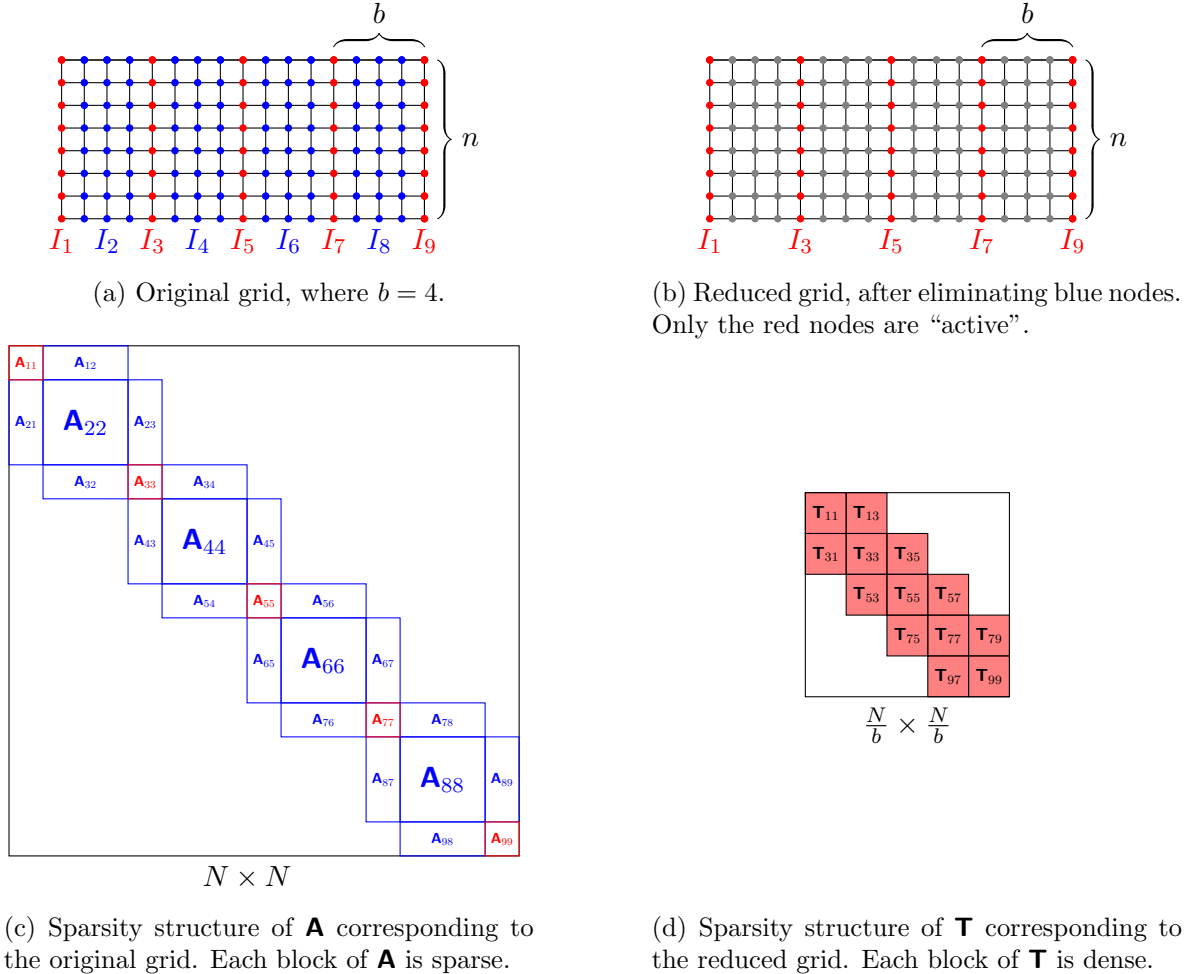


FIGURE 1

In the first stage, the nodes that are internal to each slab (identified by the index vectors I_2, I_4, \dots and shown as blue in Figure 1a) are eliminated from the linear system, resulting in the reduced problem shown in Figure 1b, with the associated coefficient matrix shown in Figure 1d. In this elimination step, we exploit that each subdomain is thin, which means that classical sparse direct solvers are particularly fast. To further accelerate this step, we use that the Schur complements that arise upon the elimination of the interior nodes are rank structured. Specifically, they are “HBS/HSS matrices” [19, 34, 35] with *exact* HBS/HSS rank at most $2b$. This allows us to accelerate this reduction step using a recently proposed randomized algorithm for compressing rank structured matrices [22].

The second stage is to factorize the remaining coefficient matrix \mathbf{T} shown in Figure 1d. This matrix is much smaller than the original matrix \mathbf{A} , but its blocks are dense. These blocks are rank structured as well, which can be exploited to reduce the asymptotic complexity of the solver. However, we have found that for 2D problems, dense operations are fast enough.

A particular advantage of the solver presented is that it is easily parallelizable, and can be accelerated via batched linear algebra and GPU computations. The numerical results demonstrate compelling speed and memory scaling, when compared to state-of-the-art sparse direct solvers. For meshes with 100 million points, the factorization can be computed in 20 minutes on a desktop with an Intel i9-12900k CPU with 16 cores and an RTX 3090 GPU. Once the factorization is available, subsequent solves take about a minute.

The scheme also interacts very well with high order discretization schemes such as those described in [28] and [26, Ch. 25], which makes it a particularly powerful tool for solving problems with highly oscillatory solutions. The numerical results feature constant and variable coefficient Helmholtz problems. Using high order discretizations, we are able to discretize the PDE to 10 points per wavelength and accurately resolve solutions on domains of size $1000\lambda \times 1000\lambda$, where λ is the wavelength, to 6 digits of relative accuracy, compared to the true solution of the PDE.

1.3. Context and Related work. Methods to solve (3) can be characterized into two groups – direct and iterative. Iterative methods have many drawbacks and challenges. In particular, the iteration count can grow substantially in the presence of ill-conditioning, and often one needs to design a preconditioner \mathbf{P} that clusters the eigenvalue spectrum of $\mathbf{P}^{-1}\mathbf{A}$. Preconditioners are often problem-specific, and for many PDEs, an efficient preconditioner is not known. For high frequency strong scattering problems with variable coefficient media, the wave may be reflected multiple times or trapped in cavities, which is challenging for known preconditioners to resolve [14, 15]. Iterative solvers can also be inefficient in situations involving multiple right hand sides or low-rank updates to \mathbf{A} .

Direct methods, which factorize \mathbf{A} exactly, offer a means of computing the solution to high accuracy without need for iteration. The solver we describe in this work is related to multi-frontal LU solvers [11]. Such solvers are particularly effective when combined with a nested dissection ordering of the grid nodes [2, 16]. For a 2D grid with N nodes, the resulting techniques have complexity $O(N^{3/2})$ to build and $O(N \log N)$ complexity to apply, which is known to be work optimal among solvers that exploit sparsity in the system only [10, 12]. Prior work in direct solvers uses rank-structured matrix representations in order to accelerate the build time of multi-frontal methods and reduce memory requirements [1, 8, 17, 36]. SlabLU also exploits rank-structures that arises in intermediate dense matrices to save on storage and efficiently construct \mathbf{T} .

SlabLU is also related to Schur complement methods, which are methods based on a non-overlapping domain decomposition with implicit treatment of the interface conditions. The interior of each subdomain is factorized in parallel; the reduced system \mathbf{T} is typically not formed but instead applied matrix-free in an iterative method [7, 29, 37]. These methods have similar advantages as SlabLU — they are easy to parallelize and involve only one global communication operation to solve \mathbf{T} . The reduced system \mathbf{T} is also better conditioned than the original system \mathbf{A} ; nevertheless, efficient preconditioners are not known for \mathbf{T} when complicated wave phenomena are present. SlabLU instead exploits the rank structure of \mathbf{T} to construct the reduced system *exactly* using a randomized sampling method and factorizes \mathbf{T} directly.

To resolve the oscillatory solutions of the Helmholtz equation, the equation must be discretized to a constant number of points per wavelength, roughly 10. PDE formulations suffer from the so-called “pollution effect” [3] — as the wavenumber increases, one may suffer from phase errors unless you discretize with *even more* points per wavelength. To combat these effects, we use a multi-domain high-order spectral collocation scheme. The discretization is a variation of the “Hierarchical Poincaré-Steklov (HPS)” scheme of [28], and our solver shares some characteristics with the one in [18]. See [26, Ch. 25] for details.

1.4. Contributions of the present work. While nested dissection techniques arrange a grid into a hierarchical quad-tree, slab-based domain decomposition techniques instead partition the grid into a number of equisized elongated domains. For purposes of building a sparse direct solver, this approach marginally increases the asymptotic flop count, but has the advantage that the slab-based decomposition is a two-level scheme that is easier to optimize. Producing the reduced system \mathbf{T} requires building direct solvers for slab subdomains in an embarrassingly parallel fashion. Factorizing \mathbf{T} , even with dense sub-blocks, can be made efficient by choosing the slab width b appropriately. Leveraging only sparsity, we achieve $O(N^{5/3})$ build time and $O(N^{7/6})$ solve time using a slab-based scheme for 2D grids. We demonstrate that simple parallel optimizations give the solver impressive practical performance on modern hybrid architectures, compared to multi-level nested dissection techniques.

A key novelty of the method described is the combination of randomized compression [22, 24, 25] with a sparse direct solver to eliminate the interior nodes in each slab. An important observation here is that the dense matrices that arise are not only approximately rank-structured, but actually have *exact* rank-deficiencies in the off-diagonal blocks, cf. Section 3.2. Importantly, these rank-deficiencies are present in the non-oscillatory and oscillatory regimes. This makes the randomized compression particularly efficient as you attain very high computational efficiency, with little loss of accuracy. The use of randomized black-box algorithms provides a purely algebraic and simple means of efficiently forming \mathbf{T} for a variety of PDE discretizations.

1.5. Limitations and extensions. SlabLU offers a compelling two-level alternative to multi-level direct methods. We demonstrate how the scheme interfaces with two different discretizations, with an emphasis on high order multidomain discretization, which is crucial to resolving complicated wave phenomena. We also discuss how SlabLU may be extended to other discretizations of rectangular domains.

The scheme may not easily extend to adaptively refined meshes or PDEs on complicated geometries. Most *hp*-refinement schemes are designed to interface with multi-frontal solvers, which are challenging to parallelize on modern hybrid architectures. SlabLU demonstrates that significant ease of computation can be gained for discretizations that are compatible with a slab decomposition by minimizing communication and exploiting parallelism.

2. DISCRETIZATION AND NODE ORDERING

We introduce two different discretization techniques for (1). The first is simply the standard second order convergent five point finite difference stencil. Since this discretization is very well known, it allows us to describe how the solver works without the need to introduce cumbersome background material. To demonstrate that the solver works for a broader class of discretization schemes, the numerical experiments reported in Section 7 also include results that rely on the high order convergent *Hierarchical Poincaré-Steklov (HPS)* scheme, which we introduce in Section 2.3.

2.1. A model problem based on the five point stencil. For purposes of describing the factorization scheme, let us introduce a very simple discretization of the boundary value problem (1).

We work with a rectangular domain $\Omega = [0, L_1] \times [0, L_2]$ and the second order linear elliptic operator \mathcal{A} defined by (2). We assume that $L_1 \geq L_2$, and that $L_1 = hn_1$ and $L_2 = hn_2$ for some grid spacing h and some positive integers n_1 and n_2 .

We then discretize \mathcal{A} with a standard second-order finite difference scheme, to obtain the linear system

$$(4) \quad \frac{1}{h^2} (\mathbf{u}(n_w) + \mathbf{u}(n_e) + \mathbf{u}(n_n) + \mathbf{u}(n_s) - 4\mathbf{u}(n)) - \kappa^2 \mathbf{b}(n)\mathbf{u}(n) = \mathbf{f}(n).$$

The vectors \mathbf{u} and \mathbf{f} are the values of the solution u and the body load f , respectively, at collocation points. See Figure 2 for a visualization of the 5 point stencil. We write the system (4) compactly as $\mathbf{A}\mathbf{u} = \mathbf{f}$.

2.2. Clustering of the nodes. We next subdivide the computational domain into thin “slabs”, as shown in Figure 1a. We let b denote the number of grid points in each slab ($b = 4$ in Figure 1a), and then introduce index vectors I_1, I_2, I_3, \dots that keep track of which slabs each grid point belongs to. The odd numbered index vectors I_1, I_3, I_5, \dots indicate nodes on the interfaces between slabs (red in Figure 1a), while the even numbered ones indicate nodes that are interior to each slab (blue in Figure 1a). With this ordering of the grid points, the stiffness matrix associated with the discretization (4) has the sparsity pattern shown in Figure 1c.

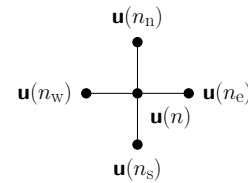


FIGURE 2. Five point stencil in 2D.

2.3. High order discretizations. The methods described in this work generalize to other discretizations of elliptic PDEs on rectangular domains, including low order finite element schemes and discontinuous Galerkin schemes. Sparse direct solvers generally do not interface well with high order schemes, as larger stencils dramatically increase fill-in [26, Ch. 25]. (For instance, the standard $O(h^4)$ accurate finite difference stencil would require that each red “mesh separator” in Figure 1a hold $3n_2$ nodes instead of n_2 nodes.) To avoid this problem, we instead rely on a high order accurate spectral collocation discretization known as the Hierarchical Poincare-Steklov scheme (HPS). This scheme was designed to interface well with sparse direct solvers so that increasing the order p does not require “widening” the separators I_1, I_3, I_5, \dots . We introduce the discretization scheme briefly; see [26, Ch. 25] for a complete discussion. The domain Ω is partitioned in non-overlapping subdomains, as shown in Figure 3. The discretization is described by two parameters a and p , which describe the subdomain “element” size and the local polynomial degree, respectively. Each subdomain has side length $2a$, and on the interior of each subdomain, the PDE is enforced via a spectral collocation scheme of order p . On the boundaries between subdomains, we enforce that the flux is continuous. On each subdomain of p^2 nodes, the interior nodes interact densely with themselves and to the boundary nodes (i.e. a dense interaction matrix of size $p^2 \times p^2$).

To improve efficiency when HPS is combined with sparse direct solvers, we “eliminate” the dense interactions of nodes interior to each subdomain. The remaining nodes are on the boundaries between subdomains, and the remaining grid has $\approx n_1 n_2 / p$ points. This process produces an equivalent stiffness matrix $\tilde{\mathbf{A}}$ with equivalent body load $\tilde{\mathbf{f}}$ on the remaining grid points. The reduced system $\tilde{\mathbf{A}}$ is block sparse, with blocks of size $p \times p$. See Figure 3 for the remaining grid, after eliminating the points interior to each subdomain. We write the equivalent system as

$$(5) \quad \tilde{\mathbf{A}}\tilde{\mathbf{u}} = \tilde{\mathbf{f}}.$$

Remark 1. A key point of the present work is that the solver has only two levels, which makes the “H” in “HPS” a slight misnomer, as it refers to “hierarchical”. We nevertheless stick with the “HPS” acronym to conform with the prior literature.

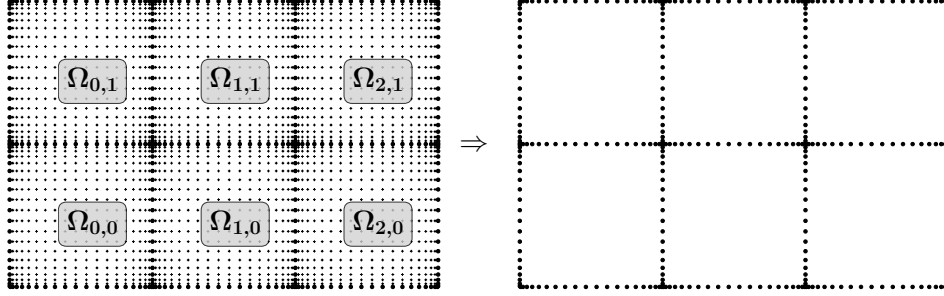


FIGURE 3. HPS is a multi-domain spectral collocation scheme that may be incompatible with sparse direct solvers due to dense interactions on the interior of each subdomain. Prior to interfacing with SlabLU, we “eliminate” the interior nodes and produce an equivalent system to solve on the boundaries. The original grid has $n_1 \times n_2$ points, and remaining grid has $\approx n_1 n_2 / p$ points.

3. STAGE ONE: ELIMINATION OF NODES INTERIOR TO EACH SLAB

This section describes the process that we use to eliminate the nodes interior to each slab that we sketched out in Section 1.2. The objective is to reduce the sparse stiffness matrix \mathbf{A} (illustrated in Figure 1c) into the smaller block tridiagonal matrix \mathbf{T} (illustrated in Figure 1d). The accelerations described form the core innovation of the manuscript.

3.1. Schur complements. With the ordering introduced in Section 2.2, the linear system \mathbf{A} has the block form

$$(6) \quad \begin{bmatrix} \mathbf{A}_{11} & \mathbf{A}_{12} & \mathbf{0} & \mathbf{0} & \mathbf{0} & \dots \\ \mathbf{A}_{21} & \mathbf{A}_{22} & \mathbf{A}_{23} & \mathbf{0} & \mathbf{0} & \dots \\ \mathbf{0} & \mathbf{A}_{32} & \mathbf{A}_{33} & \mathbf{A}_{34} & \mathbf{0} & \dots \\ \mathbf{0} & \mathbf{0} & \mathbf{A}_{43} & \mathbf{A}_{44} & \mathbf{A}_{45} & \dots \\ \vdots & \vdots & \vdots & \vdots & \vdots & \vdots \end{bmatrix} \begin{bmatrix} \mathbf{u}_1 \\ \mathbf{u}_2 \\ \mathbf{u}_3 \\ \mathbf{u}_4 \\ \vdots \end{bmatrix} = \begin{bmatrix} \mathbf{f}_1 \\ \mathbf{f}_2 \\ \mathbf{f}_3 \\ \mathbf{f}_4 \\ \vdots \end{bmatrix}.$$

We eliminate the vectors $\mathbf{u}_2, \mathbf{u}_4, \mathbf{u}_6, \dots$ that represent unknown variables in the interior of each slab through a step of block Gaussian elimination. To be precise, we insert the relation

$$(7) \quad \mathbf{u}_i = \mathbf{A}_{ii}^{-1} (\mathbf{f}_i - \mathbf{A}_{i,i-1} \mathbf{u}_{i-1} - \mathbf{A}_{i,i+1} \mathbf{u}_{i+1}), \quad i = 2, 4, 6, \dots$$

into the odd-numbered rows in (6) to obtain the reduced system

$$(8) \quad \begin{bmatrix} \mathbf{T}_{11} & \mathbf{T}_{13} & \mathbf{0} & \mathbf{0} & \mathbf{0} & \dots \\ \mathbf{T}_{31} & \mathbf{T}_{33} & \mathbf{T}_{35} & \mathbf{0} & \mathbf{0} & \dots \\ \mathbf{0} & \mathbf{T}_{53} & \mathbf{T}_{55} & \mathbf{T}_{57} & \mathbf{0} & \dots \\ \mathbf{0} & \mathbf{0} & \mathbf{T}_{75} & \mathbf{T}_{77} & \mathbf{T}_{79} & \dots \\ \vdots & \vdots & \vdots & \vdots & \vdots & \vdots \end{bmatrix} \begin{bmatrix} \mathbf{u}_1 \\ \mathbf{u}_3 \\ \mathbf{u}_5 \\ \mathbf{u}_7 \\ \vdots \end{bmatrix} = \begin{bmatrix} \tilde{\mathbf{f}}_1 \\ \tilde{\mathbf{f}}_3 \\ \tilde{\mathbf{f}}_5 \\ \tilde{\mathbf{f}}_7 \\ \vdots \end{bmatrix},$$

where the sub-blocks of \mathbf{T} are defined as

$$(9) \quad \mathbf{T}_{11} = \mathbf{A}_{11} - \mathbf{A}_{12} \mathbf{A}_{22}^{-1} \mathbf{A}_{21}$$

$$(10) \quad \mathbf{T}_{13} = \mathbf{A}_{13} - \mathbf{A}_{12} \mathbf{A}_{22}^{-1} \mathbf{A}_{23}$$

$$(11) \quad \mathbf{T}_{31} = \mathbf{A}_{31} - \mathbf{A}_{32} \mathbf{A}_{22}^{-1} \mathbf{A}_{23}$$

$$(12) \quad \mathbf{T}_{33} = \mathbf{A}_{33} - \mathbf{A}_{32} \mathbf{A}_{22}^{-1} \mathbf{A}_{23} - \mathbf{A}_{34} \mathbf{A}_{44}^{-1} \mathbf{A}_{43}$$

$$(13) \quad \mathbf{T}_{35} = \mathbf{A}_{35} - \mathbf{A}_{34} \mathbf{A}_{44}^{-1} \mathbf{A}_{43}$$

and so on. The reduced right-hand sides $\tilde{\mathbf{f}}$ are defined as

$$(14) \quad \tilde{\mathbf{f}}_1 = \mathbf{f}_1 - \mathbf{A}_{12} \mathbf{A}_{22}^{-1} \mathbf{f}_2$$

$$(15) \quad \tilde{\mathbf{f}}_3 = \mathbf{f}_3 - \mathbf{A}_{32} \mathbf{A}_{22}^{-1} \mathbf{f}_2 - \mathbf{A}_{34} \mathbf{A}_{44}^{-1} \mathbf{f}_4$$

$$(16) \quad \tilde{\mathbf{f}}_5 = \mathbf{f}_5 - \mathbf{A}_{54} \mathbf{A}_{44}^{-1} \mathbf{f}_4 - \mathbf{A}_{56} \mathbf{A}_{66}^{-1} \mathbf{f}_6$$

and so on.

3.2. Rank structure in the reduced blocks. We next discuss algebraic properties of the blocks of the reduced system \mathbf{T}_{ij} that allow for \mathbf{T} to be formed efficiently. The sub-blocks of \mathbf{T} are Schur-complements of sparse matrices. For instance, block \mathbf{T}_{11} has the formula

$$(17) \quad \mathbf{T}_{11} = \begin{matrix} \mathbf{A}_{11} & - & \mathbf{A}_{12} & \mathbf{A}_{22}^{-1} & \mathbf{A}_{21} \\ n_2 \times n_2 & & n_2 \times n_2 & n_2b \times n_2b & n_2b \times n_2 \end{matrix},$$

where $\mathbf{A}_{11}, \mathbf{A}_{12}, \mathbf{A}_{21}$ are sparse with $O(n_2)$ entries and \mathbf{A}_{22} is a sparse banded matrix. Factorizing \mathbf{A}_{22} can be done efficiently using a sparse direct solver, but applying $\mathbf{A}_{22}^{-1} \mathbf{A}_{21}$ naively may lead to a dense intermediate matrix of size $n_2b \times n_2$, which is too large to form explicitly when b is in the hundreds. There are memory-efficient means of calculating \mathbf{T}_{11} by operating on $\mathbf{A}_{12}, \mathbf{A}_{21}$ as sparse matrices, but these methods are not commonly available in sparse matrix packages and may be slow.

We use an alternate approach for efficiently forming \mathbf{T}_{11} that uses widely available sparse matrix methods; the approach achieves high arithmetic intensity while maintaining a very low memory footprint. First, we prove algebraic properties about \mathbf{T}_{11} , which is a dense but rank-structured matrix that only needs $O(n_2b)$ storage in exact precision. Then we describe how this structure can be recovered with only $O(b)$ matrix vector products (matvecs) of \mathbf{T}_{11} and \mathbf{T}_{11}^* . Matvecs can efficiently be applied because \mathbf{T}_{11} and its transpose are compositions of sparse matrices.

Proposition 3.1 (Rank Property). *Let J_B be a contiguous set of points on the slab interface J , and let J_F be the rest of the points $J_F = J \setminus J_B$. The sub-matrices $(\mathbf{T}_{11})_{BF}$, $(\mathbf{T}_{11})_{FB}$ have exact rank at most $2b$.*

See Figure 4 for an illustration of J_B . The proof is in Appendix A. This property allows \mathbf{T}_{11} to be compressible in a format called Hierarchically Block-Separable (HBS) or Hierarchically Semi-Separable (HSS) with exact HBS/HSS rank at most $2b$. HBS/HSS matrices are a type of hierarchical matrix (\mathcal{H} -matrix), which allow dense matrices to be stored efficiently by exploiting low-rank structure in sub-blocks at different levels of granularity [4, 20, 26]. The matrices \mathbf{T}_{jk} are compressible in several \mathcal{H} -matrix formats, e.g. Hierarchical Off-Diagonal Low Rank (HODLR), and can be efficiently recovered from matvecs in HODLR format as well [24, 25], though more matvecs are required for reconstruction in this format.

3.3. Recovering \mathcal{H} -matrix structure from matvecs. We next describe how to extract an \mathcal{H} -matrix representation of the reduced blocks purely from matvecs. For concreteness, we are trying to recover $\mathbf{T}_{11} \in \mathbb{R}^{n_2 \times n_2}$ as an HBS matrix with HBS rank at most $2b$. Typically, \mathcal{H} -matrices are used when the cost of forming or factorizing these matrices densely, is prohibitively large. In the context of SlabLU, $\mathbf{T}_{11} \in \mathbb{R}^{n_2 \times n_2}$ can be stored densely for the problem sizes of interest, but traditional methods for forming \mathbf{T}_{11} densely may lead to large intermediate matrices, as described in

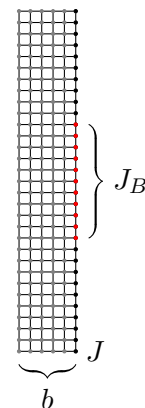


FIGURE 4. Contiguous set of points defined as $J_B \subset J$.

Section 3.2. Instead, we recover \mathbf{T}_{11} as an HBS matrix with HBS rank at most $2b$ from matrix-matrix products

$$(18) \quad \underset{n_2 \times s}{\mathbf{Y}} = \underset{n_2 \times n_2}{\mathbf{T}_{11}} \underset{n_2 \times s}{\mathbf{\Omega}}, \quad \underset{n_2 \times s}{\mathbf{Z}} = \underset{n_2 \times n_2}{\mathbf{T}_{11}^*} \underset{n_2 \times s}{\mathbf{\Psi}},$$

where $\mathbf{\Omega}, \mathbf{\Psi}$ are Gaussian random matrices and $s = 6b$ using the algorithm presented in [22]. This is theoretically possible because an HBS matrix of size $n_2 \times n_2$ with HBS rank at most $2b$ can be encoded in $O(n_2b)$ storage. The HBS structure can be recovered from samples \mathbf{Y}, \mathbf{Z} after post-processing in $O(n_2b^2)$ flops. The algorithm presented in [22] can be seen as an extension of algorithms for recovering low-rank factors from random sketches [27]. A particular advantage of these algorithms is that they scale linearly and are truly black-box. The matrix-matrix products (18) are simple to compute using the matrix-free formula (17) of \mathbf{T}_{11} and its transpose. Applying \mathbf{T}_{11} involves two applications of sparse matrices and two triangular solves using pre-computed sparse triangular factors.

3.4. Efficient factorization of the local stiffness matrices within each slab. We next describe methods to compute sparse representations of the inverses via factorization

$$(19) \quad \underset{n_2b \times n_2b}{\mathbf{A}_{22}^{-1}}, \underset{n_2b \times n_2b}{\mathbf{A}_{44}^{-1}}, \dots$$

for n_1/b sparse systems, where each system is banded with bandwidth b . The nodes in I_2 can be grouped into “supernodes” of size b , and the systems (19) can be treated as block-tridiagonal systems. There are many efficient means of paralleling the factorization of block-tridiagonal systems, especially when the blocks are relatively small [21, 31]. With small block sizes, parallel algorithms for block tridiagonal factorizations can leverage batched linear algebra (batched BLAS) routines. Traditionally, it may be challenging to achieve high arithmetic intensity for many small parallel tasks due to overhead costs; batched BLAS is a highly optimized software that groups these small inputs into larger “batches” and can achieve particularly good performance on GPUs. Batched BLAS achieves good performance when the matrices are small enough to fit in the top levels of the memory hierarchy. For matrices of larger sizes, efficient parallelism is challenging to achieve, and for large enough matrices, processing in serial is more efficient than processing them in parallel.

SlabLU is designed with the fundamental limitations to parallelism in mind. Since SlabLU is a two-level scheme, we compute factorizations of two matrix sizes — b and n_2 . The slab width b is in the hundreds, which is the regime where many small blocks can be factorized in parallel with batched BLAS. In the special case that all n_1/b systems in equation (19) have the *same* sparsity pattern, one can apply parallel operations to the same block across sparse systems. This occurs for regular discretizations on rectangular domains.

4. STAGE TWO: FACTORIZING THE REDUCED BLOCK TRIDIAGONAL SYSTEM

We next describe factorizing the reduced system \mathbf{T} in order to solve

$$(20) \quad \mathbf{T}\tilde{\mathbf{u}} = \tilde{\mathbf{f}},$$

where \mathbf{T} is a block-tridiagonal system of size roughly $N/b \times N/b$. The formulas for sub-blocks of \mathbf{T} are written in equations (9 - 13) and the equivalent body load $\tilde{\mathbf{f}}$ in equations (14 - 16). Once the reduced system \mathbf{T} is formed, Stage Two involves factorizing \mathbf{T} with $\approx n_1/b$ dense sub-blocks of size $n_2 \times n_2$. For the discretizations and problem sizes considered in this work, the factorization can be efficiently computed with GPU-accelerated BLAS. Each block \mathbf{T}_{jk} occupies at most 1GB when stored in double precision, and the LU factorization of block can be computed in 10 seconds or less on GPU.

Algorithm 1 outlines a very simple sweeping algorithm, where each block is factorized in serial. Note we only need to store n_1/b Schur complements $\mathbf{S}_1, \mathbf{S}_2, \dots$ densely to apply the

factorization to solve the system (20). One can store the off-diagonal blocks in low-memory form as HBS/HSS or as a composition of sparse matrices as in equations (10,11,13). There are alternate means of factorizing \mathbf{T} using \mathcal{H} -matrix algebra, and this is a compelling avenue for future research for larger problem sizes or for the purpose of reducing the overall memory footprint for the direct solver. Surprisingly, using dense linear algebra to factorize \mathbf{T} leads to impressive scaling for substantially large 2D grids, as we show in the numerical results.

Algorithm 1: Sweeping factorization

```

1 Given block tridiagonal system  $\mathbf{T}$ , factorize the system.
2  $\mathbf{S}_1 \leftarrow \mathbf{T}_{11}$ ;
3 for  $j = 2, \dots, n_1/b$  do
4    $\mathbf{S}_{2j+1} \leftarrow \mathbf{T}_{2j+1,2j+1} - \mathbf{T}_{2j+1,2j-1} \mathbf{S}_{2j-1}^{-1} \mathbf{T}_{2j-1,2j+1}$ ;
5   Store  $\mathbf{S}_{2j-1}^{-1}$ ;
6 Given body load  $\tilde{\mathbf{f}}$ , compute the solution  $\tilde{\mathbf{u}}$ .
7  $\mathbf{y}_1 \leftarrow \mathbf{S}_1^{-1} \tilde{\mathbf{f}}_1$ ;
8 for  $j = 1, \dots, n_1/b$  do
9    $\mathbf{y}_{2j+1} \leftarrow \mathbf{S}_{2j+1}^{-1} (\tilde{\mathbf{f}}_{2j+1} - \mathbf{T}_{2j+1,2j-1} \mathbf{y}_{2j-1})$ ;
10  $\tilde{\mathbf{u}}_{2n_1/b+1} \leftarrow \mathbf{S}_{2n_1/b+1}^{-1} \mathbf{y}_{2n_1/b+1}$ ;
11 for  $j = n_1/b, n_1/b - 1, \dots, 1$  do
12    $\tilde{\mathbf{u}}_{2j-1} \leftarrow \mathbf{S}_{2j-1}^{-1} (\mathbf{y}_{2j-1} - \mathbf{T}_{2j-1,2j+1} \tilde{\mathbf{u}}_{2j+1})$ ;

```

5. COMPLEXITY ANALYSIS

We next discuss the complexity of the method. We have left the buffer size b generic up to this point, but now we will choose b as a function of the number of grid points $N = n_1 n_2$. Stage One and Stage Two have different polynomial dependencies on b, n_1 , and n_2 . Choosing b appropriately allows us to balance costs and achieve competitive complexities for the build and solve times. The discussion on choosing b focuses on the 5-point stencil model problem, but the conclusions are generally applicable to other discretizations.

After analyzing the complexity of the build stage, we describe how to use the factorization to solve systems. We also discuss interfacing SlabLU with HPS discretizations of local polynomial order p and analyze the costs with pre-factors in p .

5.1. Choosing the buffer size b . The buffer size is chosen to balance the costs of Stage One and Stage Two. Stage One involves factorizing n_1/b sparse systems (19), where each sparse system is has block tridiagonal structure discussed in Section 3.4. Computing factorizations (19) requires $\frac{n_1}{b} \times O(b^3 n_2)$ flops.

In order to construct the reduced system \mathbf{T} , we need an efficient means of computing sparse Schur complements of the form (17). We show that the blocks \mathbf{T}_{jk} have a rank property in Proposition 3.1, which allows us to reconstruct block \mathbf{T}_{jk} using a random sampling method, as discussed in Section 3.3. The matrix-matrix products (18) for a block \mathbf{T}_{jk} can be constructed in $O(n_2 b^3)$ time using matrix-free formulas for applying \mathbf{T}_{jk} . Recovering HBS/HSS structure in \mathbf{T}_{jk} from the random samples requires $O(n_2 b^2)$ time. To summarize, Stage One is dominated by the costs of the factorizations of sparse systems (19) and constructing random samples (18), which both have costs $\frac{n_1}{b} \times O(n_2 b^4) = O(b^3 N)$. Importantly, Stage One can be done in parallel for n_1/b sub-domains and can also leverage efficient batched BLAS routines for small fronts of size $b \times b$.

Stage Two involves a simple sweeping factorization of \mathbf{T} using Algorithm 1. The reduced system \mathbf{T} has $\approx n_1/b$ blocks, each of size $n_2 \times n_2$. The total cost of constructing the factorization is

$$(21) \quad T_{\text{build}} = \underset{\text{Stage One}}{O(b^2 N)} + \underset{\text{Stage Two}}{O\left(\frac{1}{b} n_1 n_2^3\right)}.$$

To balance the costs of Stage One and Stage Two, we choose $b = O(n_2^{2/3})$. The total cost of the build stage is $T_{\text{build}} = O(n_1 n_2^{7/3}) = O(N^{5/3})$ when $n_1 = n_2$.

5.2. Applying the factorization to solve systems. We next discuss how to use the factorization to solve (3), as well as the memory costs of storing the factorization. In order to apply Algorithm 2, we need to store the sparse factorizations (19) and the factorization of \mathbf{T} . The sparse factorizations (19) require $O(\frac{n_1}{b} \times b^2 n_2)$ storage, and storing the factorization of \mathbf{T} requires $O(\frac{n_1}{b} \times n_2^2)$ storage. With the choice of $b = O(n_2^{2/3})$, the sparse factorizations require asymptotically more space to store. We can rebalance the memory costs of Stage One and Stage Two by “discarding” some of the factorization in Stage One (e.g. corresponding to small subdomains) and re-factorizing as needed to apply Algorithm 2. Then the memory costs are $T_{\text{solve}} = \frac{n_1}{b} \times O(n_2^2) = O(N^{7/6})$ when $n_1 = n_2$. Refactorizing discarded blocks of the factorization does not significantly impact the solve time since small systems can be refactorized embarrassingly in parallel; this is demonstrated in the numerical results.

Algorithm 2: Solving $\mathbf{A}\mathbf{u} = \mathbf{f}$ using factorization.	
1 Calculate equivalent body $\tilde{\mathbf{f}}$ on I_1, I_3, \dots using (14-16).	// in parallel
2 Solve $\mathbf{T}\tilde{\mathbf{u}} = \tilde{\mathbf{f}}$ for $\tilde{\mathbf{u}}$ on I_1, I_3, \dots using Algorithm 1.	// serial algorithm
3 Solve for \mathbf{u} on I_2, I_4, \dots using $\tilde{\mathbf{u}}$ on I_1, I_3, \dots using (7).	// in parallel

5.3. Interfacing HPS with sparse direct solvers. We discuss constant prefactors in the build and solve stage when factorizing systems (3) for HPS discretizations. For many discretizations, increasing the local polynomial order p leads to large constant pre-factors with p in the build and solve costs for a sparse factorization. This is because increasing p often leads to needing to “widen” separators I_1, I_3, \dots to find subdomains I_2, I_4, \dots that can be factorized in parallel; see the sparsity pattern of \mathbf{A} in Figure 1c.

We discuss in Section 2.3, interfacing HPS discretizations with SlabLU requires an elimination of the leaf nodes to produce a reduced system $\tilde{\mathbf{A}}$. Producing $\tilde{\mathbf{A}}$, which is of size roughly $N/p \times N/p$, requires $O(p^4 N)$ ops. When the buffer size b is chosen as prescribed in Section 5.1, then the overall complexity of SlabLU remains the same, with no prefactor dependence on p when factorizing $\tilde{\mathbf{A}}$ with SlabLU. The prefactor dependence on p only appears in the cost of producing $\tilde{\mathbf{A}}$. Though $O(p^4 N)$ scaling appears prohibitively expensive, the prefactor is not visible in the timing results reported in Section 7 for $p = 22$. The leaf operations can be done in an embarrassingly parallel fashion with batched BLAS and further accelerated on a GPU.

6. REDUCING COMMUNICATION AND EXPLOITING PARALLELISM

We next discuss practical performance concerns relating to parallelizing sparse direct solvers for PDEs discretized on rectangular grids. We highlight properties of the SlabLU that make the scheme particularly simple to optimize on modern hybrid architectures. We also discuss

why such optimizations are challenging to implement for parallel multi-level nested dissection codes.

6.1. Parallelism and GPU Acceleration in SlabLU. SlabLU is a two-level scheme, which only requires factorizing two front sizes — b in Stage One and n_2 in Stage Two. Stage One requires factorizing n_1/b sparse systems (19) in parallel, each with sub-blocks of size $b \times b$. This task is parallelized with batched BLAS, which is a software framework for efficiently executing independent BLAS operations on many small matrices. Such parallel operations are further accelerated on GPUs, a high-throughput architecture; see Section 3.4.

The dense sub-blocks of \mathbf{T} are challenging to form using classical methods, as discussed in Section 3.2; instead, we recover \mathbf{T}_{jk} as HBS/HSS from random samples (18) using matrix-free formulas (17). Applying \mathbf{T}_{jk} to $O(b)$ vectors involves two applications of sparse matrices and two triangular solves using pre-computed sparse triangular factors. This involves BLAS3 operations on small sub-blocks and can be accelerated on GPUs with batched BLAS. The samples for each block \mathbf{T}_{jk} can also be produced in parallel.

In Stage Two, factorizing \mathbf{T} using Algorithm (1) leverages the efficiency of BLAS3 operations on dense matrices of size $n_2 \times n_2$. For N up to 100M, the sub-blocks of \mathbf{T} can be efficiently factorized in a few seconds on a GPU. With n_1/b sub-blocks in \mathbf{T} , setting b to grow as $b = O(n_2^{2/3})$ keeps the size of \mathbf{T} manageable as N grows. Slab-based solvers also provide a general framework that allows for \mathbf{T} to be factorized using \mathcal{H} -matrix algebras, for which GPU acceleration with batched BLAS has been of interest [6, 9].

6.2. Challenges in Parallelizing Nested Dissection. The nested dissection ordering leads to a work-optimal factorization by minimizing fill-in in the computed factorization. Parallelizing such codes and making efficient use of powerful architectures remains an active area of research. Sparse direct solvers rely on BLAS3 computational kernels (e.g. factorization, triangular matrix-vector solvers, rank- k update matrix multiplication). These kernels, in and of themselves, are highly efficient on modern architectures and can benefit from GPU acceleration. In practice, traversing multi-level trees is a memory-bound operation that is challenging to substantially accelerate [30, 33].

At every level of the tree, the subtasks are of different sizes. Batched linear algebra offers substantial acceleration for parallel operations on many small matrices, and BLAS3 operations on a single dense matrix can be accelerated as well. For many parallel operations on intermediate-sized matrices, it is challenging to assign threads to subtasks. The tree structure may also demand CPU-driven coordination, necessitating moving data from GPU to CPU at every level of the tree.

7. NUMERICAL EXPERIMENTS

We next demonstrate the effectiveness of the solver through numerical experiments. We report build time, as well as solve time and accuracies for a variety of constant and variable-coefficient elliptic PDEs using two different discretizations. The experiments scale to 100M points, with the largest problem size requiring less than 20 minutes to factorize. The experiments are run on a desktop with a 16-core Intel i9-12900k CPU with 128GB of memory and a NVIDIA RTX 3090 GPU with 24GB of memory. We have chosen to run the experiments on a high-powered desktop, rather than on a large-memory node, to demonstrate that the solver can be efficiently built with a reasonable memory footprint.

The discretizations used are (1) 2nd order finite difference and a (2) high-order multi-domain spectral collocation scheme, known as the HPS scheme. The former is commonly used as a simple discretization to demonstrate the effectiveness of novel solvers, but it suffers from the pollution effect. As a result, the Helmholtz equation has to be discretized to 100-250 points per wavelength in order to avoid $O(1)$ phase errors for large problem sizes. Increasing

the local polynomial order p helps to combat the effects of pollution; we use HPS, a high-order scheme that interfaces particularly well with sparse direct solvers, as discussed in Sections 2.3 and 5.3.

The first subsection includes experiments for both discretizations, to demonstrate that SlabLU has competitive timings and memory scalings. The PDEs in this subsection have known solutions; we report relative accuracy in the residual as well as relative accuracy with respect to the known solution. In the presence of ill-conditioning in the PDE, SlabLU is able to resolve solutions to high accuracy. The build times and memory footprint compare favorably to SuperLU, which is a state-of-the-art nested dissection solver.

The second subsection uses HPS with high local polynomial order to solve challenging scattering phenomena for variable-coefficient PDEs. SlabLU is able to resolve the solutions to high accuracy in the residual of the PDE, even in the presence of variable coefficients. Importantly, we can discretize the Helmholtz equation to 10 points per wavelength, without the effect of pollution. The largest problem of $N=100M$ points corresponds to a physical domain 1000 wavelengths wide.

7.1. Experiments for PDEs with known solutions. We next demonstrate how the solver performs on PDEs with manufactured or analytically calculated solutions for two different discretizations. The first PDE (22) is the Poisson equation with nonzero body load. The second PDE (24) is the constant coefficient Helmholtz equation. The latter PDE is highly ill-conditioned, and solving the discretized equation accurately requires LU with partial pivoting. This is a challenge for SlabLU, which only allows for row permutations within the same block; the reported accuracies demonstrate that SlabLU can calculate accurate solutions despite this limitation.

We show competitive scalings for the build time of the factorization and for the memory footprint. Despite the super-linear complexity scaling, the scaling appears to be linear for grids of size up to $N=100M$. For coercive PDEs, there is rarely a reason to scale the discretizations to such large grids. For the Helmholtz equation, discretizing to at least 10 points per wavelength is necessary to resolve the oscillatory solutions, leading to large grids. Direct solvers are especially compelling for the Helmholtz equation because many scattering problems are outside the reach of iterative methods.

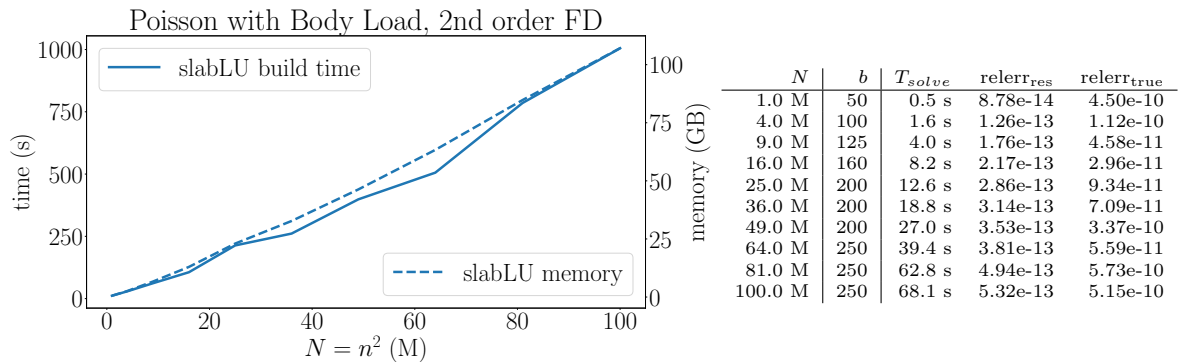


FIGURE 5. Timing results for solving Poisson equation with a body load (eq. 22) using a 2nd order finite difference discretization. Though the build time of SlabLU scales as $O(N^{5/3})$, the observed asymptotic behavior has linear scaling with N .

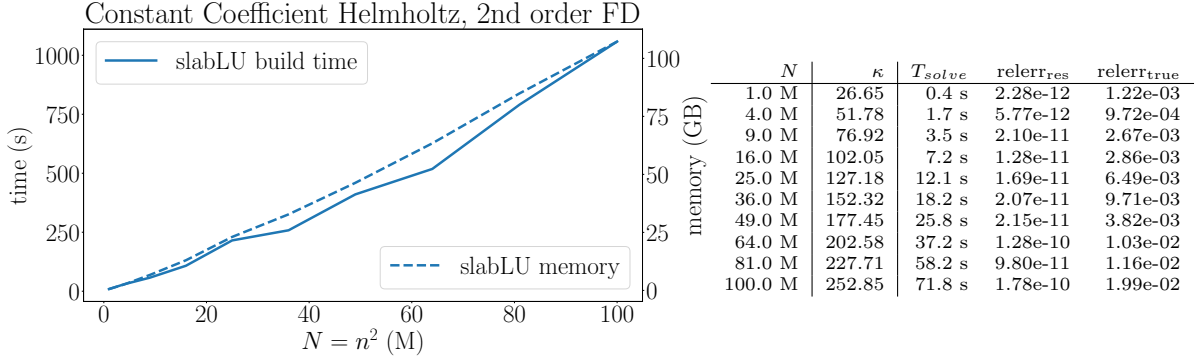


FIGURE 6. Timing results for solving the constant coefficient Helmholtz equation (eq. 24) using a 2nd order finite difference discretization. The wavenumber κ is increased with the problem size to maintain 250 points per wavelength. Though the solution is resolved to at least 10 digits in the residual, the relative error compared to the true solution is only 3 digits.

7.1.1. *Description of PDEs and Accuracies Reported.* The first PDE considered is a Poisson problem with a body load

$$(22) \quad \begin{cases} -\Delta u(x) = f(x), & x \in \Omega, \\ u(x) = u_{\text{true}}(x), & x \in \Gamma, \end{cases}$$

The Dirichlet data is the restriction of the true analytic solution to the boundary

$$(23) \quad u_{\text{true}}(x) = (c_1 - x_1)^2(c_1 + x_1)^2 + (c_2 - x_2)^2(c_2 + x_2)^2,$$

where c_1, c_2 are nonzero constants. The body load f is given by applying the Laplace operator to the known solution u_{true} . The second PDE considered is a constant coefficient Helmholtz problem

$$(24) \quad \begin{cases} -\Delta u(x) - \kappa^2 u(x) = 0, & x \in \Omega, \\ u(x) = u_{\text{true}}(x), & x \in \Gamma, \end{cases}$$

where the true solution u_{true} is given by

$$(25) \quad u_{\text{true}} = J_0(\kappa \|x - (-0.1, 0.5)\|),$$

where $x \mapsto J_0(\kappa|x|)$ is the free-space fundamental solution to the Helmholtz equation.

Upon applying the direct solver, we obtain the calculated solution \mathbf{u}_{calc} at discretization points interior to the domain. We report relative error with respect to the residual of the discretized system (3) and with respect to the true solution \mathbf{u}_{true} evaluated at the collocation points

$$(26) \quad relerr_{\text{res}} = \frac{\|\mathbf{A}\mathbf{u}_{\text{calc}} - \mathbf{f}\|_2}{\|\mathbf{f}\|_2}, \quad relerr_{\text{true}} = \frac{\|\mathbf{u}_{\text{calc}} - \mathbf{u}_{\text{true}}\|_2}{\|\mathbf{u}_{\text{true}}\|_2}.$$

7.1.2. *Solving high frequency Helmholtz equations with SlabLU.* Sparse direct solvers use sparsity in the discretized operators in order to factorize the system exactly. SlabLU uses sparsity in the traditional sense for the sparse factorizations (19) in Stage One. In order to construct the reduced system \mathbf{T} , we prove a rank property in Proposition (3.1) that allows us to represent sub-blocks $\mathbf{T}_{jk} \in \mathbb{R}^{n_2 \times n_2}$ exactly in $O(n_2 b)$ storage and recover \mathbf{T}_{jk} in HBS/HSS format using random sampling; see Section 3.3. Crucially, Proposition (3.1) is a purely algebraic property that holds regardless of the PDE. The numerical results for FD and HPS discretizations demonstrate that construction of \mathbf{T} using random sampling does not cause substantial

loss of accuracy in the residual of the discretized Helmholtz equation; see Figures 6 and 8. Due to the pollution effect, Helmholtz experiments using 2nd order FD require discretizing the equation to 100-250 points per wavelength to achieve 2-3 digits of relative accuracy with respect to the true solution. In contrast, the HPS discretization with $p = 22$ does not appear to suffer from the pollution effect and can accurately resolve oscillatory solutions using 10 points per wavelength. The effect of pollution is very stark for low order discretizations. The largest problem discretized with FD of size $N=100$ M corresponds to a square domain of 40 wavelengths. The smallest problem discretized with HPS of 1M points corresponds to a domain of 50 wavelengths.

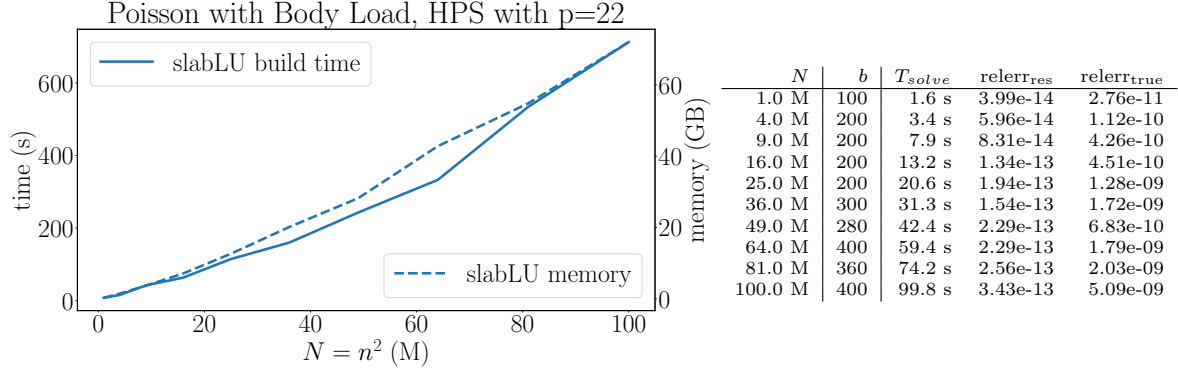


FIGURE 7. Timing results for solving Poisson equation with a body load (eq. 22) using an HPS discretization with $p = 22$. The presence of a body load means that we must solve a local problem on the leaf nodes to find the equivalent body load on “reduced” grid, but this operation does not significantly impact solve time. Though the build time of SlabLU scales superlinearly, the observed asymptotic behavior has linear scaling with N .

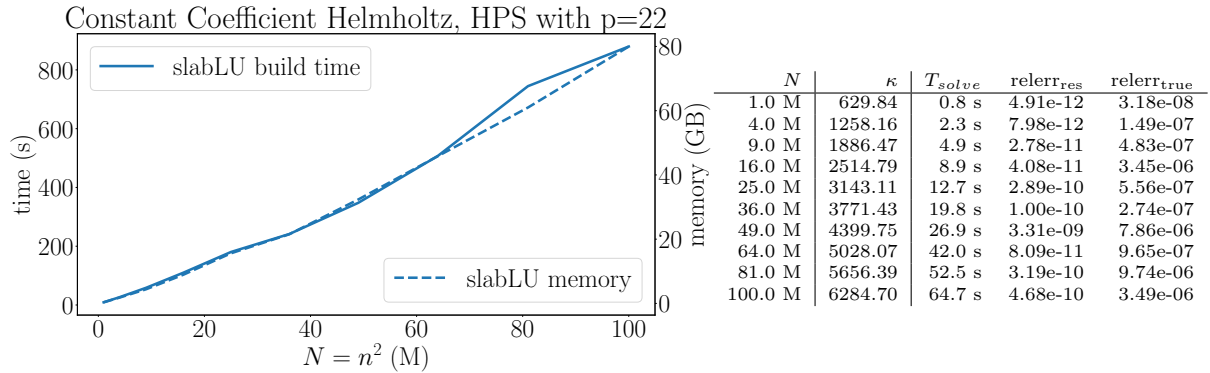


FIGURE 8. Timing results for solving the constant coefficient Helmholtz equation (eq. 24) using an HPS discretization with $p = 22$. The wavenumber κ is increased with the problem size to maintain 10 points per wavelength. Using a high order multidomain spectral collocation scheme allows us to avoid the effects of pollution and achieve at least 5 digits of relative accuracy, compared to the known solution.

Often, the HBS/HSS rank of \mathbf{T}_{jk} is considerably less than $2b$; SlabLU uses adaptive rank sampling in the HBS/HSS construction to considerably save on build time and storage costs. For a thin slab with λ wavelengths in the thin dimension, we have observed that the ranks are roughly twice λ plus a constant factor. For the Poisson equation, HBS/HSS rank about

50 approximates \mathbf{T}_{jk} to high accuracy. Compare Figures 7 and 8 to see that there are slightly higher build times and memory costs for the Helmholtz equation discretized with HPS.

7.1.3. Solve Times and Memory Costs. In order to improve efficiency when HPS is combined with sparse direct solvers, we remove the interior leaf nodes from the system, as discussed in Section 2.3, to produce an equivalent system $\tilde{\mathbf{A}}\tilde{\mathbf{u}} = \tilde{\mathbf{f}}$. Calculating the equivalent body load $\tilde{\mathbf{f}}$ and the solution on the full HPS grid both require $O(p^4N)$ operations; see Section 5.3. The leaf information is discarded to reduce the memory footprint of the overall solver and re-computed as needed. The solve times reported for HPS include the time needed for leaf computations; the leaf operations for $p = 22$ are extremely efficient and require less than a minute for the problem sizes considered.

We briefly discuss the differences in the memory footprint and solve times for FD and HPS. The FD discretization does not discard any parts of the factorization; whereas, HPS does discard leaf factorizations and regenerate them as needed. As a result, the largest factorization for (22) with the HPS discretization has a memory footprint of 50GB, whereas the same PDE discretized with FD requires more than 100GB to store; see Figures 5 and 7. There are clear trade-offs between storing more information and re-computing pieces of the factorization as needed for the solve time. Surprisingly, the solve times for HPS are not much higher than the solve times for FD; small systems can be re-factorized in parallel with batched BLAS and GPU acceleration.

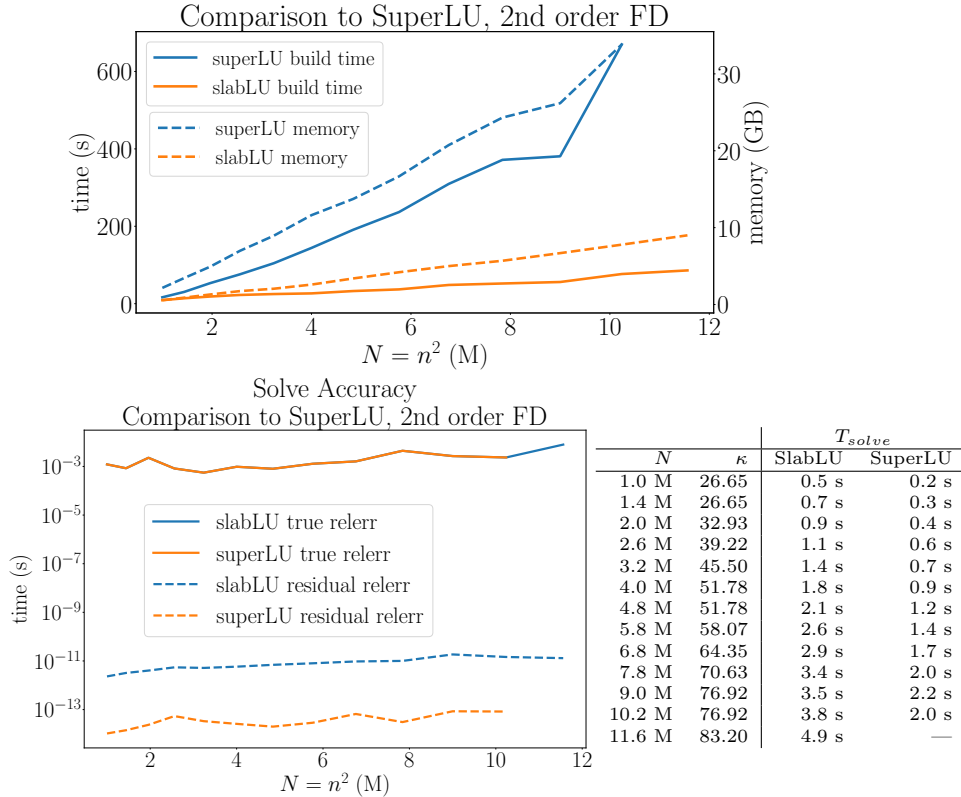


FIGURE 9. Comparison to Super LU for 2d order FD. SlabLU groups nodes into supernodes to leverage batched BLAS3 operations in Stage One and uses GPU acceleration for the large fronts in Stage Two. The SlabLU factorization time is faster by a factor of 8 and more memory efficient by a factor of 4 for $N = 10.2$ M.

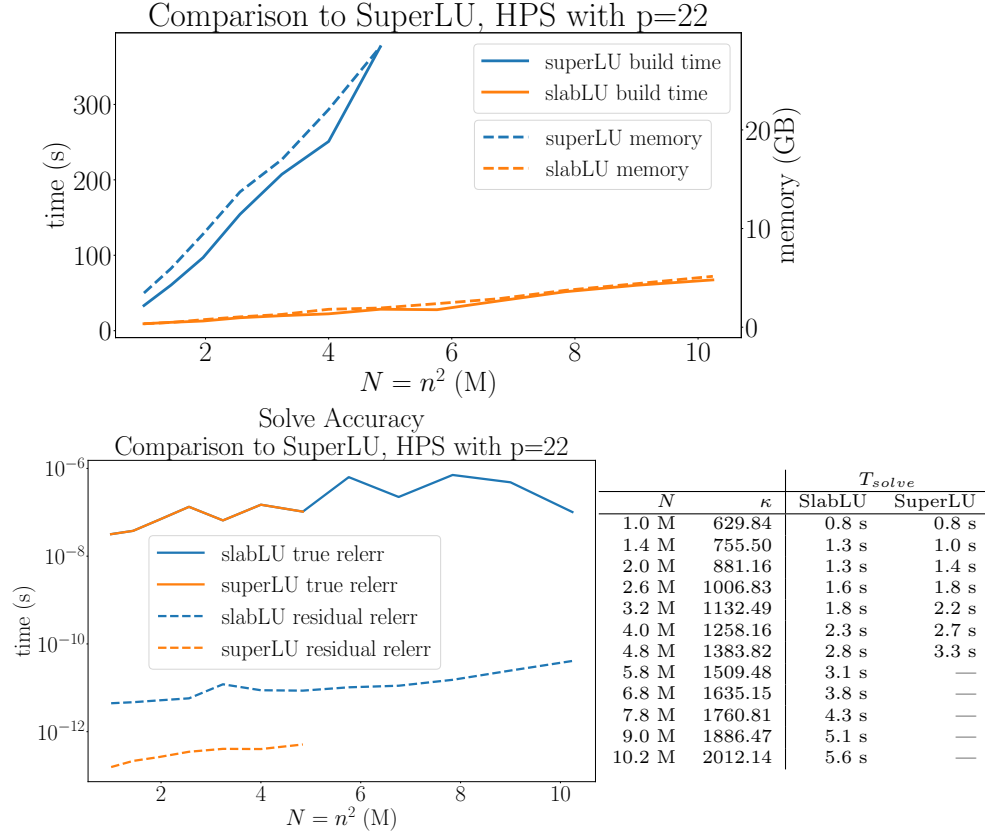


FIGURE 10. Comparison to SuperLU for HPS with $p = 22$. As discussed in Section 2.3, we form a reduced system $\tilde{\mathbf{A}}$ roughly of size $N/p \times N/p$ and factorize $\tilde{\mathbf{A}}$ using sparse direct solvers. The time needed to form $\tilde{\mathbf{A}}$ is included in the build time. SlabLU factorization time is faster by a factor of 12 and more memory efficient by a factor of 14 for $N=4.8\text{M}$. The Helmholtz equation is discretized to 10 points per wavelength and is highly ill-conditioned. SuperLU is able to factorize the system with better relative accuracy in the residual; however, both SlabLU and SuperLU solve the equations to the same relative accuracy, compared to the true PDE solution.

7.2. Comparison to SuperLU. We next report direct comparisons between SlabLU and SuperLU for two different discretizations. For these comparisons, we discretize the constant coefficient Helmholtz equation (24), which leads to very ill-conditioned sparse systems (3) to solve. SuperLU is a generic sparse direct solver that can compute a sparse LU factorization of any given sparse matrix to high accuracy using groupings of nodes into “supernodes” to leverage BLAS3 operations on dense sub-blocks [5, 23]. We call SuperLU via the Scipy interface (version 1.8.1) and use the default permutation specification of COLAMD ordering. SuperLU does include steps which are not present in the SlabLU, which impact the overall build time of SuperLU. Prior to factorization, SuperLU finds the matrix ordering that minimizes fill-in and finds sub-blocks that can be grouped into supernodes to leverage BLAS3 operations. During the factorization, SuperLU may pivot between sub-blocks in order to achieve stability in the computed factorization; as a result, SuperLU can achieve superior accuracy in the residual. Despite limitations in the pivoting scheme of SlabLU, both schemes resolve the solution up to the discretization error; see Figures 9 and 10. The comparison demonstrates that SlabLU outperforms SuperLU on build times and memory costs up to about 10M points. For larger

problems, SuperLU does not compute the factorization, likely because the memory footprint would exceed some pre-prescribed limit.

7.3. Variable-coefficient PDEs. We next demonstrate the ability of SlabLU to solve complicated scattering phenomena. To be precise, we solve BVP (1) with the variable-coefficient Helmholtz operator (2) and discretize using HPS with $p = 22$, which does not suffer from the pollution effect; see Figure 8. The problems physically correspond to an antenna releasing an electromagnetic signal in a closed room, which is an important but challenging physical phenomenon to simulate. As discussed in Section 1.2, preconditioners are often tailored to particular PDEs and boundary conditions, and no efficient preconditioner is known for wave phenomena with multiple reflections and trapped rays. These phenomena are induced by Dirichlet boundary data, because wave cannot escape the closed domain.

The Dirichlet data u_{dir} for the experiments in this section is given by a Gaussian pulse on the left boundary of the domain

$$(27) \quad u_{\text{dir}}(x) = \begin{cases} \exp(-2000(x_1 - 0.5)^2), & \text{when } x_0 = 0 \\ 0, & \text{otherwise.} \end{cases}$$

We consider a variety of scattering media b which satisfy $0 \leq b(x) \leq 1$.

b_0 : constant coefficient

b_1 : photonic crystal shown in Figure 12

b_2 : photonic crystal with corner-shaped waveguide in Figure 13

In the absence of an analytic solution, we rely on the residual to confirm that we have solved the equations accurately; see Figure 11 for a table of residual errors for variable-coefficient PDEs with Dirichlet data u_{dir} . The presence of variable coefficients does not affect the SlabLU build time, memory footprint, or solve time; see Figure 8 which shows this information for (24) discretized at 10 points per wavelength using HPS with $p = 22$.

N	κ	relerr _{res}		
		b_0	b_1	b_2
1.0 M	629.84	4.91e-12	1.41e-10	4.20e-10
4.0 M	1258.16	7.98e-12	6.88e-09	8.83e-09
9.0 M	1886.47	2.78e-11	3.43e-09	7.88e-09
16.0 M	2514.79	4.08e-11	1.61e-09	1.03e-08
25.0 M	3143.11	2.89e-10	6.35e-09	5.88e-09
36.0 M	3771.43	1.00e-10	2.29e-08	1.15e-08
49.0 M	4399.75	3.31e-09	1.91e-08	4.53e-08
64.0 M	5028.07	8.09e-11	2.64e-07	2.51e-07
81.0 M	5656.39	3.19e-10	3.78e-08	2.72e-07
100.0 M	6284.70	4.68e-10	2.50e-08	2.84e-08

FIGURE 11. For the HPS discretization for $p = 22$, this table shows residual errors for various scattering fields b and Dirichlet data u_{dir} . The wavenumber is increased with N to maintain a constant 10 ppw. Comparing the residual errors for variable fields b_1 and b_2 to the constant field b_0 , we do not see much loss of accuracy in the residual due to the presence of variable coefficients.

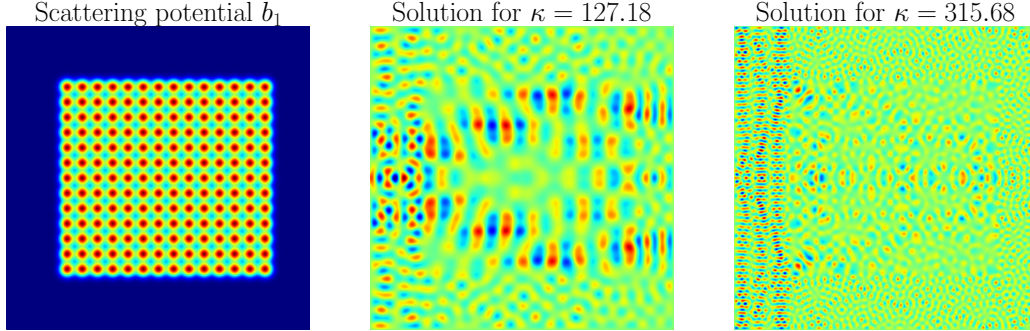


FIGURE 12. Solutions for Dirichlet data u_{dir} with scattering field b_1 discretized using HPS with $p = 22$ on a grid of 1M points. The photonic crystal blocks the pulse originating on the left boundary from reaching the right boundary.

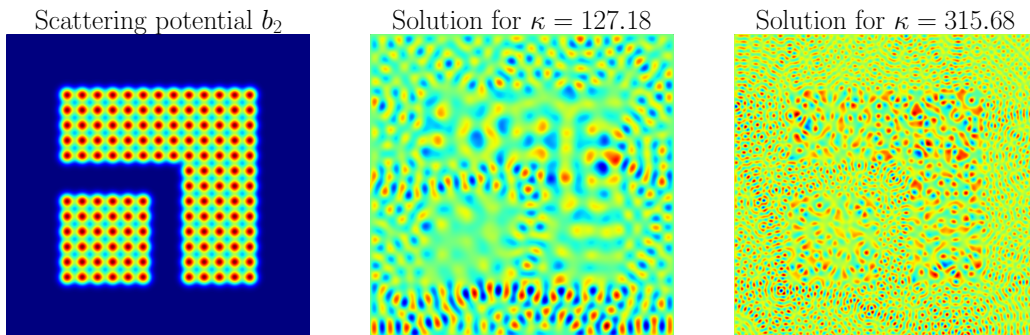


FIGURE 13. Solutions for Dirichlet data u_{dir} with scattering field b_2 discretized using HPS with $p = 22$ on a grid of 1M points. The pulse originating at the left boundary can propagate through the corner waveguide. Such physical phenomena are archetypically challenging to simulate.

8. CONCLUSION

This paper presents SlabLU, a sparse direct solver framework for elliptic PDEs on rectangular domains. SlabLU decomposes the domain into a sequence of thin slabs. The degrees of freedom internal to each slab are eliminated in parallel, yielding a reduced system \mathbf{T} defined on the slab interfaces. The reduced system \mathbf{T} is factorized directly. A key novelty of the method is the use of randomized compression with a sparse direct solver to efficiently form \mathbf{T} . The dense sub-blocks of \mathbf{T} have *exact* rank deficiencies in the off-diagonal blocks that are present in the non-oscillatory and oscillatory regimes. The use of randomized black-box algorithms provides a purely algebraic means of efficiently forming \mathbf{T} for a variety of PDE discretizations. SlabLU requires $O(N^{5/3})$ time to build and $O(N^{7/6})$ time to apply. The general two-level framework is simple to implement, easy to parallelize, and can be accelerated via batched linear algebra and GPU computations. SlabLU interfaces well with high order multi-domain spectral collocation schemes, allowing for the rapid and accurate simulation of challenging scattering phenomena.

The authors are in the process of extending the SlabLU methodology to solve challenging physical phenomena in 3D. For 3D problems, the reduced matrix \mathbf{T} is too large to form densely and must be formed and factorized using \mathcal{H} -matrix algebra. Thin 3D slabs have exact rank deficiencies that allow for the sub-blocks of \mathbf{T} to be formed efficiently via randomized sampling. The challenge, is that the ranks in 3D are considerably larger than for 2D problems, and sampling thin 3D slabs effectively requires the development of a novel randomized scheme.

APPENDIX A. RANK PROPERTY OF THIN SLABS

In this appendix, we prove Proposition 3.1, which makes a claim on the rank structure of \mathbf{T}_{11} , defined in (17).

Proposition 3.1 (Rank Property). *Let J_B be a contiguous set of points on the slab interface J , and let J_F be the rest of the points $J_F = J_1 \setminus J_B$. The sub-matrices $(\mathbf{T}_{11})_{BF}$, $(\mathbf{T}_{11})_{FB}$ have exact rank at most $2b$.*

Recall that $\mathbf{T}_{11} = \mathbf{A}_{11} - \mathbf{A}_{12}\mathbf{A}_{22}^{-1}\mathbf{A}_{21}$. The proof relies on the sparsity structure of the matrices in the Schur complement. As stated in the proposition, I_1 is partitioned into indices I_B and I_F . The proof relies on partitioning I_2 as well, into the indices $I_\alpha, I_\beta, I_\gamma$ shown in Figure 14, where $|I_\gamma| = 2b$.

The matrix $\mathbf{A}_{2,2}$ is sparse and can be factorized as

$$(28) \quad \mathbf{A}_{2,2} = \mathbf{L}_{2,2}\mathbf{U}_{2,2} := \begin{bmatrix} \mathbf{L}_{\alpha\alpha} & & \\ & \mathbf{L}_{\beta,\beta} & \\ \mathbf{L}_{\gamma,\alpha} & \mathbf{L}_{\gamma,\beta} & \mathbf{L}_{\gamma,\gamma} \end{bmatrix} \begin{bmatrix} \mathbf{U}_{\alpha,\alpha} & & \mathbf{U}_{\alpha,\gamma} \\ & \mathbf{U}_{\beta,\beta} & \mathbf{U}_{\beta,\gamma} \\ & & \mathbf{U}_{\gamma,\gamma} \end{bmatrix}$$

The formula for $(\mathbf{T}_{1,1})_{F,B}$ can be re-written as

$$(29) \quad (\mathbf{T}_{1,1})_{F,B} = \mathbf{A}_{F,B} - (\mathbf{A}_{F,2}\mathbf{U}_{2,2}^{-1})(\mathbf{L}_{2,2}^{-1}\mathbf{A}_{2,B}) := \mathbf{A}_{F,B} - \mathbf{X}_{F,2} \mathbf{Y}_{2,B}$$

The factors $\mathbf{X}_{F,2}$ and $\mathbf{Y}_{2,B}$ have sparse structure, due the sparsity in the factorization (28) and the sparsity of $\mathbf{A}_{F,2}$ and $\mathbf{A}_{2,B}$.

$$(30) \quad \mathbf{X}_{F,2} = [\mathbf{A}_{F,\alpha} \quad 0 \quad \mathbf{A}_{F,\gamma}] \mathbf{U}_{2,2}^{-1}, \quad \mathbf{Y}_{2,B} = \mathbf{L}_{2,2}^{-1} \begin{bmatrix} 0 \\ \mathbf{A}_{\beta,B} \\ \mathbf{A}_{\gamma,B} \end{bmatrix}$$

The factors $\mathbf{X}_{F,2}$ and $\mathbf{Y}_{2,B}$ have the same sparsity pattern as $\mathbf{A}_{F,2}$ and $\mathbf{A}_{2,B}$, respectively. As a result,

$$(31) \quad (\mathbf{T}_{1,1})_{F,B} = \mathbf{A}_{F,B} - [\mathbf{X}_{F,\alpha} \quad 0 \quad \mathbf{X}_{F,\gamma}] \begin{bmatrix} 0 \\ \mathbf{Y}_{\beta,B} \\ \mathbf{Y}_{\gamma,B} \end{bmatrix} = \begin{matrix} \mathbf{A}_{F,B} \\ \text{sparse, } O(1) \text{ entries} \end{matrix} - \begin{matrix} \mathbf{X}_{F,\gamma} \mathbf{Y}_{\gamma,B} \\ \text{exact rank } 2b \end{matrix}.$$

Similar reasoning can be used to show the result for $(\mathbf{T}_{11})_{B,F}$.

REFERENCES

- [1] Patrick Amestoy, Alfredo Buttari, Jean-Yves l'Excellent, and Theo Mary. On the complexity of the block low-rank multifrontal factorization. *SIAM Journal on Scientific Computing*, 39(4):A1710–A1740, 2017.
- [2] Patrick R Amestoy, Timothy A Davis, and Iain S Duff. An approximate minimum degree ordering algorithm. *SIAM Journal on Matrix Analysis and Applications*, 17(4):886–905, 1996.
- [3] Ivo M Babuska and Stefan A Sauter. Is the pollution effect of the fem avoidable for the helmholtz equation considering high wave numbers? *SIAM Journal on numerical analysis*, 34(6):2392–2423, 1997.
- [4] Mario Bebendorf. *Hierarchical matrices*, volume 63 of *Lecture Notes in Computational Science and Engineering*. Springer-Verlag, Berlin, 2008. A means to efficiently solve elliptic boundary value problems.
- [5] Matthias Bollhöfer, Olaf Schenk, Radim Janalik, Steve Hamm, and Kiran Gullapalli. State-of-the-art sparse direct solvers. In *Parallel Algorithms in Computational Science and Engineering*, pages 3–33. Springer, 2020.
- [6] Wajih Boukaram, George Turkiyyah, and David Keyes. Hierarchical matrix operations on gpus: Matrix-vector multiplication and compression. *ACM Transactions on Mathematical Software (TOMS)*, 45(1):1–28, 2019.
- [7] Luiz Mariano Carvalho, Luc Giraud, and Patrick Le Tallec. Algebraic two-level preconditioners for the schur complement method. *SIAM Journal on Scientific Computing*, 22(6):1987–2005, 2001.

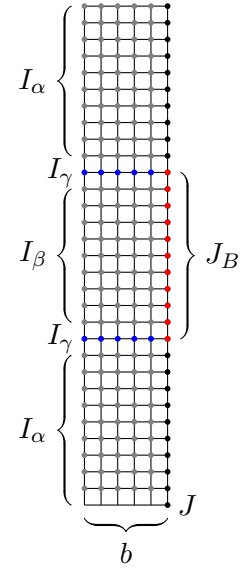


FIGURE 14

- [8] Gustavo Chávez, George Turkiyyah, Stefano Zampini, Hatem Ltaief, and David Keyes. Accelerated cyclic reduction: A distributed-memory fast solver for structured linear systems. *Parallel Computing*, 74:65–83, 2018.
- [9] Chao Chen and Per-Gunnar Martinsson. Solving linear systems on a gpu with hierarchically off-diagonal low-rank approximations. *arXiv preprint arXiv:2208.06290*, 2022.
- [10] Timothy A Davis. *Direct methods for sparse linear systems*, volume 2. Siam, 2006.
- [11] Timothy A. Davis, Sivasankaran Rajamanickam, and Wissam M. Sid-Lakhdar. A survey of direct methods for sparse linear systems. *Acta Numerica*, 25:383 – 566, 2016.
- [12] I.S. Duff, A.M. Erisman, and J.K. Reid. *Direct Methods for Sparse Matrices*. Oxford, 1989.
- [13] Björn Engquist and Lexing Ying. Sweeping preconditioner for the helmholtz equation: hierarchical matrix representation. *Communications on pure and applied mathematics*, 64(5):697–735, 2011.
- [14] Oliver G Ernst and Martin J Gander. Why it is difficult to solve helmholtz problems with classical iterative methods. *Numerical analysis of multiscale problems*, pages 325–363, 2012.
- [15] Martin J Gander and Hui Zhang. Restrictions on the use of sweeping type preconditioners for helmholtz problems. In *International Conference on Domain Decomposition Methods*, pages 321–332. Springer, 2017.
- [16] A. George. Nested dissection of a regular finite element mesh. *SIAM J. on Numerical Analysis*, 10:345–363, 1973.
- [17] P. Ghysels, X. Li, F. Rouet, S. Williams, and A. Napov. An efficient multicore implementation of a novel hss-structured multifrontal solver using randomized sampling. *SIAM Journal on Scientific Computing*, 38(5):S358–S384, 2016.
- [18] A. Gillman and P. Martinsson. A direct solver with $o(n)$ complexity for variable coefficient elliptic pdes discretized via a high-order composite spectral collocation method. *SIAM Journal on Scientific Computing*, 36(4):A2023–A2046, 2014. arXiv.org report #1307.2665.
- [19] Adrianna Gillman, Patrick Young, and Per-Gunnar Martinsson. A direct solver $o(n)$ complexity for integral equations on one-dimensional domains. *Frontiers of Mathematics in China*, 7:217–247, 2012. 10.1007/s11464-012-0188-3.
- [20] Wolfgang Hackbusch. *Hierarchical matrices: algorithms and analysis*, volume 49. Springer, 2015.
- [21] Hee-Seok Kim, Shengzhao Wu, Li-wen Chang, and W Hwu Wen-mei. A scalable tridiagonal solver for gpus. In *2011 International Conference on Parallel Processing*, pages 444–453. IEEE, 2011.
- [22] James Levitt and Per-Gunnar Martinsson. Linear-complexity black-box randomized compression of hierarchically block separable matrices. *arXiv preprint arXiv:2205.02990*, 2022.
- [23] Xiaoye S Li and Meiyue Shao. A supernodal approach to incomplete lu factorization with partial pivoting. *ACM Transactions on Mathematical Software (TOMS)*, 37(4):1–20, 2011.
- [24] L. Lin, J. Lu, and L. Ying. Fast construction of hierarchical matrix representation from matrix-vector multiplication. *Journal of Computational Physics*, 230(10):4071 – 4087, 2011.
- [25] Per-Gunnar Martinsson. Compressing rank-structured matrices via randomized sampling. *SIAM Journal on Scientific Computing*, 38(4):A1959–A1986, 2016.
- [26] Per-Gunnar Martinsson. *Fast Direct Solvers for Elliptic PDEs*, volume CB96 of *CBMS-NSF conference series*. SIAM, 2019.
- [27] Per-Gunnar Martinsson and Joel A Tropp. Randomized numerical linear algebra: Foundations and algorithms. *Acta Numerica*, 29:403–572, 2020.
- [28] P.G. Martinsson. A direct solver for variable coefficient elliptic pdes discretized via a composite spectral collocation method. *Journal of Computational Physics*, 242(0):460 – 479, 2013.
- [29] Yousef Saad and Maria Sasonkina. Distributed schur complement techniques for general sparse linear systems. *SIAM Journal on Scientific Computing*, 21(4):1337–1356, 1999.
- [30] Piyush Sao, Richard Vuduc, and Xiaoye Sherry Li. A distributed cpu-gpu sparse direct solver. In *European Conference on Parallel Processing*, pages 487–498. Springer, 2014.
- [31] Ioannis E Venetis, Alexandros Kouris, Alexandros Sobczyk, Efstratios Gallopoulos, and Ahmed H Sameh. A direct tridiagonal solver based on givens rotations for gpu architectures. *Parallel Computing*, 49:101–116, 2015.
- [32] Alexandre Vion, R Bélanger-Rioux, L Demanet, and Christophe Geuzaine. A ddm double sweep preconditioner for the helmholtz equation with matrix probing of the dtn map. *Mathematical and Numerical Aspects of Wave Propagation WAVES*, 2013, 2013.
- [33] Richard Vuduc, Aparna Chandramowlishwaran, Jee Choi, Murat Guney, and Aashay Shringarpure. On the limits of gpu acceleration. In *Proceedings of the 2nd USENIX conference on Hot topics in parallelism*, volume 13, 2010.
- [34] Shen Wang, Xiaoye S Li, Jianlin Xia, Yingchong Situ, and Maarten V De Hoop. Efficient scalable algorithms for solving dense linear systems with hierarchically semiseparable structures. *SIAM Journal on Scientific Computing*, 35(6):C519–C544, 2013.

- [35] J. Xia, S. Chandrasekaran, M. Gu, and X.S. Li. Fast algorithms for hierarchically semiseparable matrices. *Numerical Linear Algebra with Applications*, 17(6):953–976, 2010.
- [36] Jianlin Xia, Shivkumar Chandrasekaran, Ming Gu, and Xiaoye S. Li. Superfast multifrontal method for large structured linear systems of equations. *SIAM J. Matrix Anal. Appl.*, 31(3):1382–1411, 2010.
- [37] Fuzhen Zhang. *The Schur complement and its applications*, volume 4. Springer Science & Business Media, 2006.